

3-31-2023

## CABLE DECOUPLING AND CABLE-BASED STIFFENING OF CONTINUUM ROBOTS

Parsa Molaei

*Louisiana State University and Agricultural and Mechanical College*

Follow this and additional works at: [https://digitalcommons.lsu.edu/gradschool\\_theses](https://digitalcommons.lsu.edu/gradschool_theses)



Part of the [Acoustics, Dynamics, and Controls Commons](#)

---

### Recommended Citation

Molaei, Parsa, "CABLE DECOUPLING AND CABLE-BASED STIFFENING OF CONTINUUM ROBOTS" (2023).  
*LSU Master's Theses*. 5720.

[https://digitalcommons.lsu.edu/gradschool\\_theses/5720](https://digitalcommons.lsu.edu/gradschool_theses/5720)

This Thesis is brought to you for free and open access by the Graduate School at LSU Digital Commons. It has been accepted for inclusion in LSU Master's Theses by an authorized graduate school editor of LSU Digital Commons. For more information, please contact [gradetd@lsu.edu](mailto:gradetd@lsu.edu).

# **CABLE DECOUPLING AND CABLE-BASED STIFFENING OF CONTINUUM ROBOTS**

A Thesis

Submitted to the Graduate Faculty of the  
Louisiana State University and  
Agricultural and Mechanical College  
in partial fulfillment of the  
requirements for the degree of  
Master of Science in Mechanical Engineering

in

The Department of Mechanical & Industrial Engineering

by

Parsa Molaei

B.S., Sharif University of Technology, 2018

May 2023

”There exists a field, beyond all  
notions of right and wrong. I will meet  
you there.”

—Rumi

## Acknowledgments

I would first like to thank my supervisor, Dr. Hunter Gilbert for his guidance, patience, and support, without him this work would not have been possible. I would also like to thank Dr. Marcio de Queiroz and Dr. Corina Barbalata for agreeing to serve as my committee members. Lastly, I would like to thank all my labmates and co-workers who helped me along this path.

# Table of Contents

Acknowledgments . . . . .	iii
List of Tables . . . . .	v
List of Figures . . . . .	vi
Abstract . . . . .	vii
Chapter 1. Introduction . . . . .	1
1.1. Background . . . . .	1
1.2. Medical applications . . . . .	2
1.3. Space applications . . . . .	2
1.4. Relation to the state of the art . . . . .	5
Chapter 2. Mathematical and Physical Modelings . . . . .	9
2.1. Modeling background and assumptions . . . . .	9
2.2. Preliminaries . . . . .	11
2.3. Perfect cable decoupling . . . . .	13
2.4. Approximate cable decoupling . . . . .	14
Chapter 3. Experimental Validations . . . . .	21
3.1. Cable stiffening design considerations . . . . .	21
3.2. Prototype design . . . . .	23
3.3. Kinematic simulations . . . . .	26
3.4. Prototype stiffness measurements . . . . .	28
Chapter 4. Discussion . . . . .	33
Chapter 5. Conclusion . . . . .	35
Appendix A. Kinematic Simulations MATLAB Code . . . . .	36
Appendix B. Publication Information . . . . .	39
Bibliography . . . . .	40
Vita . . . . .	43

## List of Tables

3.1. Prototype robot design parameters. . . . .	23
3.2. Prototype cable support locations and radii. . . . .	23

## List of Figures

1.1. Behavior of a cable-driven continuum robot under a transverse gravity loading .	8
2.1. Cable shapes for example of orthogonal modes . . . . .	17
3.1. Flowchart describing the design approach . . . . .	22
3.2. Prototype exploded view and motion sequence . . . . .	24
3.3. Topology optimization result of cable supports . . . . .	25
3.4. Topology optimized 3D printed cable supports . . . . .	25
3.5. Simulation of constant curvature bending of the backbone . . . . .	27
3.6. Force and displacement data captured . . . . .	29
3.7. Prototype stiffness measurements results . . . . .	31
3.8. Experimental setup for stiffness characterization . . . . .	32

## Abstract

<sup>1</sup> Cable-driven continuum robots, which are robots with a continuously flexible backbone and no identifiable joints that are actuated by cables, have shown great potential for many applications in unstructured, uncertain environments. However, the standard design for a cable-driven continuum robot segment, which bends a continuous backbone along a circular arc, has many compliant modes of deformation which are uncontrolled, and which may result in buckling or other undesirable behaviors if not ameliorated. In this study, a detailed approach for using additional cables to selectively stiffen planar cable-driven robots without substantial coupling to the actuating cables is investigated. A mechanics-based model based on the planar Cosserat equations is used to find the design conditions under which additional cables can be routed without coupling of the cable lengths for small deformations. Simulations show that even for relatively large deformations, coupling remains small. A prototype was designed and evaluated, and it was demonstrated that the compliance of the robot is substantially modified relative to the same robot without the additional stiffening cables. The additional stiffening cables are shown to increase the end-effector output stiffness by a factor of approximately 10 over a typical design with actuating cables.

---

<sup>1</sup>Some portions of the abstract was previously published as: "Molaei, P., Pitts, N. A., Palardy, G., Su, J., Mahlin, M. K., Neilan, J. H., Gilbert, H. B. (2022). Cable Decoupling and Cable-Based Stiffening of Continuum Robots. IEEE Access, 10, 104852-104862."



# Chapter 1. Introduction

## 1.1. Background

A tendon-driven continuum robot is inspired by slender animals such as snakes and octopus tentacles [1] and it is composed of a flexible and elastic component that contains multiple tendon guides and tendons itself, which are utilized to manipulate and deform the structure of the robot body, also called the backbone, by pulling on the tendons and applying tension on them [8]. The use of tendon-driven robots and other similar high-degree-of-freedom structures has been explored extensively for various purposes such as minimally invasive surgery [2], [3], space application and manipulation [4], nuclear inspection and testing [5], and general manipulation tasks in unstructured environments [6]. The ability to actuate the tendons remotely, helps to keep designs compact and to facilitate lightweight mechanisms that are beneficial in space- and mass-constrained applications. The soft robot's flexible and elastic backbone offers certain advantages over conventional and traditional manipulators with numerous physical joints, particularly in densely packed environments, where the elasticity of the robot structure enables it to respond well to its uncertain surroundings [7]. The elastic compliance could be beneficial to ensure safe interactions with the unpredictable surrounding environment and protect both the robot and its workspace. A well-designed continuum robot should utilize its structural and design properties to attain flexibility, control, accessibility, reliability, and most importantly, structural stability.

## 1.2. Medical applications

Continuum robotic manipulators and their precursors consisting of high DoF hyper-redundant mechanisms have always been investigated as a suitable choice for medical applications such as minimally invasive surgery and endoscopy. Tendon-driven soft/continuum robots and many other flexible continuum mechanics, because of their inherited compliance and the capability to function in unpredictable, uncertain, and complex environments, have been increasingly proposed and investigated previously for a variety of medical applications such as Otolaryngology and vascular and cardiac surgery, where the continuum robot would either enter the patient's body through one of the natural orifices or a minimally incision performed by the surgeon [9], [10]. Although in most of the medical cases flexibility and safe interaction with the patient's body is required, some surgical procedures such as bone milling or osteolysis do in fact require higher device rigidity and stiffness to perform the task properly [11].

## 1.3. Space applications

<sup>1</sup> Human space exploration is an essential mission of the National Aeronautics and Space Administration (NASA). The development of large and sustainable structures in space and for planetary habitats has been identified as one of the key enabling technologies as the next strategic thrust in space technology advancement. Various in-space assembly technologies have been developed for making large space assets at NASA Langley Research Center. A cable-driven compliant space robotic technology has demonstrated

---

<sup>1</sup>Some portions of Section 1.3 were previously published as: "Molaei, P., Pitts, N. A., Palardy, G., Su, J., Mahlin, M. K., Neilan, J. H., Gilbert, H. B. (2022). Cable Decoupling and Cable-Based Stiffening of Continuum Robots. IEEE Access, 10, 104852-104862."

unique capabilities and advantages in terms of flexibility, durability, and remote adjustability. The performance of the system can be optimized by the design of configuration and the selection of cable materials through modeling and experimental validation. Advancing human space exploration entails developing larger and more sustainable structures in space and on other worlds requiring in-space manufacturing, assembly, and servicing. Identified as the next strategic thrust for NASA, In-space Assembly Servicing and Manufacturing (ISAM) offers key possibilities by freeing a mission from the restrictions of mass and volume of current launch vehicles. It is also crucial to consider how to optimize assembly methods and agents being used to diversify what capabilities they must allow for a broad range of applications, minimizing launch cost. NASA Langley Research Center’s (LaRC) in-space assembly and autonomy researchers have been developing various technology capabilities required to make larger space assets. For example, in 2002, LaRC’s Automated Telescope Assembly Lab (ASAL) autonomously assembled and disassembled an 8-meter truss structure [12]. Recently research in in-space assembly has been ramping up with NASA funding technology development for three tipping point In-Space Robotic Manufacturing and Assembly (IRMA) projects, Dragon-fly [13], Archinaut [14], and the Commercial Infrastructure for Robotic Assembly and Servicing (CIRAS) [15]. In Addition, the NASA in-Space Assembled Telescope (iSAT) Study recommended to the 2020 Astronomy and Astrophysics Decadal Survey that ISA be considered as a possible enabling method for future large space telescopes for its risk, cost, and science benefits [16]. In this effort, cable-driven systems have been developed, highlighted by the “Tendon-Actuated Lightweight In Space MANipulator” (TALISMAN) developed by LaRC. TALISMAN was created to address the deficiencies in the current state of the art in long reach manipu-

lators by utilizing an antagonistic tendon design [4]. TALISMAN simplified joint design and enhanced mechanical advantage by removing the motors from the joints themselves and reduced the size and power requirements for the overall control train. The system improved operational robustness, active antagonistic control, and reduced motor torque requirements [4]. The work also proved the case for cable-driven manipulation systems for in-space assembly and servicing operations. Compliant robotic systems provide unique capabilities and advantages regarding the space environment. Less rigid structures are more difficult to damage, resulting in a more robust system. This is crucial for environments that are far from human contact and influence. A more durable and robust system allows for decision making with an incomplete information set. This decreases risk and increases the system’s capability with respect to exploring unknown environments. Thus far, research in this area has focused on mobility for exploration, muscular assistance, and human space suit augmentation. For surface exploration, Yale’s TT-3 [17] and JPL’s tumbleweed [18] ball have used the concept of tensegrity and inflatables respectively as novel methods of traversing difficult and unknown surface conditions. Omniskins [19] are adaptable skins that can be wrapped around various objects (e.g. Rocks) giving them the potential for mobility. For liquid environments such as Jupiter’s Moon Europa, which is believed to host water oceans under its surface, Cornell has explored a squid like robot referred to as Roboel [20]. Additionally, human space suits resist astronaut mobility, significantly increasing fatigue and limiting extravehicular activity (EVA) duration. Augmenting human motion with soft actuators inside a suit is an active area of research. Shape memory alloy (NiTi – muscle wire) has been investigated as an additional tendon embedded in a suit to assist in joint mobility [21]. However, cable-driven systems, more specifically,

continuum systems, have the advantage of an infinite number of degrees of freedom (DOF) such that they can theoretically bend at any position along the length of the manipulator. This characteristic affords the manipulator the ability to work in confined spaces and in environments that can be both unknown and complex. This makes cable-driven continuum robotic manipulators of great interest for in-space assembly operations both on-orbit and on planetary surfaces where neither full human presence nor knowledge of the surface can be guaranteed.

#### 1.4. Relation to the state of the art

<sup>2</sup> Research on technologies and techniques to achieve the right balance between "too rigid" and "too flexible" has been ongoing for both rigid-link manipulators and continuum or hyper-redundant manipulators and having adjustable stiffness have always been considered a beneficial option [22] when navigating through tortuous spaces [23]. For example, in laparoscopic surgery the flexibility of the robotic mechanism is desirable in order to reach the target spot in the patients body without damaging the pathway and then when the surgeon wants to operate and remove some of the damaged tissue, the added weight would require a stiffer and more capable robot to be able to lift and remove the extra weight. Figure 1.1 shows a typical cable-driven continuum manipulator with an actuating cable located at a fixed radius to a slender elastic backbone and pulled to change the length of the cable and therefore the shape of the robot. A transverse gravity loading is applied at the end-effector, and the deformation shown occurs because of the loading. De-

---

<sup>2</sup>Some portions of Section 1.4 were previously published as: "Molaei, P., Pitts, N. A., Palardy, G., Su, J., Mahlin, M. K., Neilan, J. H., Gilbert, H. B. (2022). Cable Decoupling and Cable-Based Stiffening of Continuum Robots. IEEE Access, 10, 104852-104862."

spite a fixed cable displacement, the stiffness at the end-effector remains relatively low because unactuated modes of deformation exist which do not stretch the cable, and the elastic backbone provides nearly all the stiffness along these modes. Generally, a low output stiffness is beneficial for safety, but it also accompanies a reduction in accuracy and force output capability. However, in the context of ISAM, precise and forceful manipulation will sometimes be required. Although the elastic structure could be made stiffer, this is not always desirable, since doing so loses some of the benefits of a compliant manipulator and causes a greater tension to be developed in the actuating cables. Therefore, a simple strategy to increase output stiffness without affecting the basic kinematics and operation of the robot, either at design time or during operation of the robot, is highly desirable. Other approaches to stiffening or reducing a continuum robot’s flexibility along unactuated degrees of freedom have been studied. These approaches include granular jamming and other forms of locking using friction or mechanical interference, and phase changing materials which vary their elastic properties [24]. These approaches all work via increasing the overall elastic body stiffness rather than by selectively modifying only the stiffness along the unactuated degrees of freedom. The result is that once these technologies are activated, the robot is no longer able to undergo large deformations along the desired, actuated mode of motion. Our cable-stiffening approach does not have this limitation. Prior works have considered how the choice of the cable route affects the mechanics of continuum structures and have proposed the use of many actuators and cables to gain more control over the output stiffness and robot shape, but the question of whether multiple cables can be decoupled to control independent degrees of freedom (e.g., bending, compound bending, twisting, etc.) has not been answered to date. Unlike lower-mobility cable-driven

platform robots, which use cables to constrain degrees of freedom without actuating them [25], cable-driven continuum robots additionally involve the direct coupling of cables with elastic structures undergoing large deformations, preventing the direct application of existing approaches. Mechanics-based models for general cable routing in continuum robots are known [26], [27], and we use these prior modeling approaches in our analysis. It is known that cable paths which cross over the backbone can be used to create “S” shapes in continuum robots and that various cable routing strategies can reduce coupling between independent joints in multi-joint continuum robots [28]. It is also known that both the cable path relative to the backbone and the stiffness of the cable against changes in length has a large effect on the observable stiffness and loading behavior of the robot. In addition, cable paths which converge or diverge from the elastic backbone produce large changes in the stiffness distribution, and the behavior under prescribed cable tension (low cable stiffness), vs. prescribed cable displacement (high cable stiffness), is fundamentally different [29]. However, the full space of potential cable paths remains largely unexplored. No state-of-the-art methods to design non-trivial cable paths for simultaneous and uncoupled control of multiple elastic degrees of freedom are known. Our contribution in this paper is to present a novel design concept along with the supporting mechanics-based analysis that enables more complete control of the shape and stiffness of continuum manipulators without requiring large numbers of actuators and real-time models to compensate for the natural coupling of multiple cables. The new approach satisfies the identified need of modifying output stiffness without substantially affecting the basic kinematics and operation of the robot. To enable the approach, we identify a new design condition in the form of a nonlinear differential equation, the solutions to which are specially designed cable paths.

We focus solely on planar designs in this initial work for the sake of clarity, but the theory can be and will be extended to spatially actuated robots in future works. To demonstrate and validate the feasibility of the proposed idea, we present a prototype with two cables that independently actuate a circular bending mode and stiffen an unactuated compound bending mode. An initial constant curvature-based simulation on the backbone of the manipulator was conducted to illustrate the weak coupling between the change of the actuating and stiffening cables lengths. We demonstrate experimentally that the robot bends in circular curves without slacking of the stiffening cables, and the output end-effector stiffness is improved by a factor of 10 via the addition of the secondary set of cables. The distribution of stiffness along the robot’s length is measured and shown to be fundamentally modified by the introduction of a second set of cables.

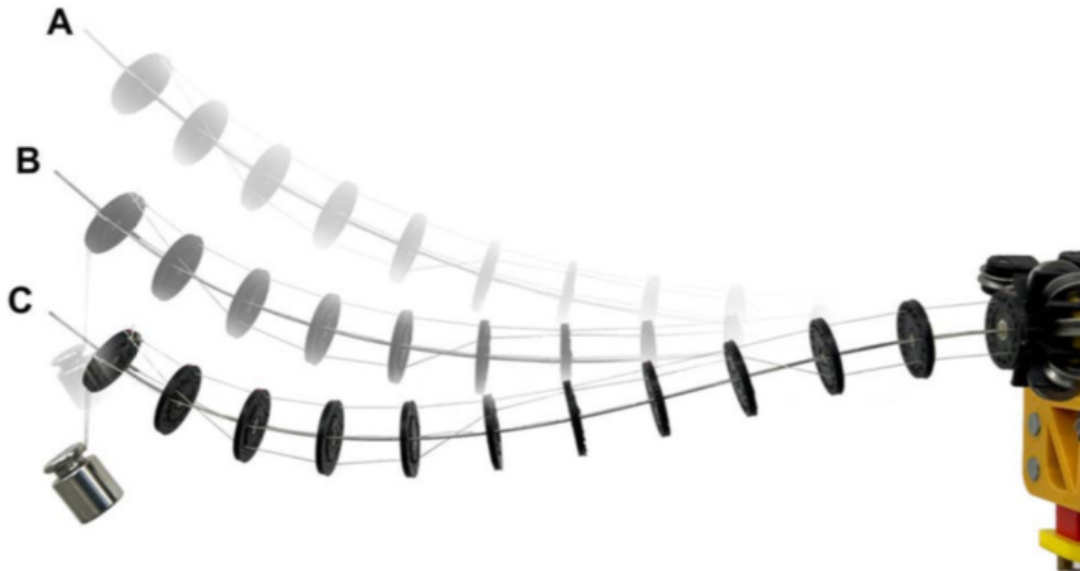


Figure 1.1. Behavior of a cable-driven continuum robot with a traditional straight tendon routing under a transverse gravity loading. The underactuated nature of the system is seen explicitly as load increases with a fixed cable displacement. A. Cable-driven continuum robot under only self-weight in a cantilevered configuration. B. Robot under an additional 10 g gravity loading at the end-effector. C. Robot under a 20 g gravity loading.



## Chapter 2. Mathematical and Physical Modelings

### 2.1. Modeling background and assumptions

<sup>1</sup> Our modeling approach follows the Cosserat-rod based approach of Rucker *et al.* [26] and also incorporates the modal shape function approach of Chirikjian and Burdick [30]. The shape of the robot is assumed to be modeled by a single planar curve which is parameterized by arc length. The position of the neutral axis of the slender backbone, with respect to a fixed frame of reference, is denoted  $\vec{p} : D \rightarrow E^3$  where  $D = [0, L]$ , and  $L$  is the length of the robot. The independent arc length variable is  $s \in D$ . The curve is framed by the addition of an arc-length parameterized frame of reference  $F(s)$  having origin  $\vec{p}(s)$  and orthogonal director vectors  $\vec{d}_1(s)$  tangent to the curve and  $\vec{d}_2$  and  $\vec{d}_3$  spanning the cross sections normal to the curve. The following modeling assumptions are adopted:

- A1. The cross sections normal to the backbone curve remain planar and do not deform (Euler-Bernoulli bending hypothesis).
- A2. The path of the  $i$ th cable is described by a vector-valued function  $\vec{r}_i(s)$ , where the cable position is:

$$\vec{p}_i(s) = \vec{p}(s) + \vec{r}_i(s) \tag{1}$$

and the vector  $\vec{r}_i$  is stationary with respect to changes in the configuration when

---

<sup>1</sup>Some portions of Section 2.1 were previously published as: "Molaei, P., Pitts, N. A., Palardy, G., Su, J., Mahlin, M. K., Neilan, J. H., Gilbert, H. B. (2022). Cable Decoupling and Cable-Based Stiffening of Continuum Robots. IEEE Access, 10, 104852-104862."

measured in the frame of reference  $F(s)$ . In other words,

$$\vec{r}_i(s) = r_{i2}(s)\vec{d}_2(s) \quad (2)$$

A3. The cables are perfectly inextensible.

A4. The function  $r_{i2}$  is differentiable with respect to  $s$ .

A5. The internal moment is linearly related to the local curvature  $\kappa(s)$  as

$$m(s) = k_b(s)\kappa(s) \quad (3)$$

A6. The robot shape is planar, and the backbone position and director vectors satisfy the following kinematic hypotheses implying that shear and extension are negligible

$$\frac{d\vec{d}_k}{ds} = \vec{\kappa} \times \vec{d}_k \quad (4)$$

$$\frac{d\vec{p}}{ds} = \vec{d}_1 \quad (5)$$

$$\vec{\kappa}(s) = \kappa(s) \times \vec{d}_3(s) \quad (6)$$

A7. The curvature  $\kappa(s)$  is assumed to be differentiable.

A8. The reference, stress-free configuration of the backbone is straight.

## 2.2. Preliminaries

*Definition 1:* The energy inner product is the bilinear form  $\langle \cdot, \cdot \rangle : V \times V \rightarrow \mathbb{R}$  is defined by:

$$\langle a, b \rangle_{k_b} = \frac{1}{2} \int k_b(\sigma) a(\sigma) b(\sigma) d\sigma \quad (7)$$

*Definition 2:* The energy norm is given by:

$$\|\kappa\|_{k_b} = \langle \kappa, \kappa \rangle \quad (8)$$

*Definition 3:* An orthonormal basis  $B$  is given:

$$B = \{\phi_k \mid k = 1, \dots, \infty\} \quad (9)$$

such that,

$$\langle \phi_i, \phi_k \rangle_{k_b} = \delta_{ik} \quad (10)$$

where  $\delta_{ik}$  is the Kronecker delta.

Then, we may write the curvature as a sum of weighted curvature modes:

$$\kappa(s) = \sum_{n=1}^{\infty} q_i \phi_i(s) \quad (11)$$

*Definition 4:* Each of the normalized basis functions  $\phi_i$  is called a curvature mode.

A finite approximation to the sum suffices for engineering purposes. Therefore, the configuration space  $\mathcal{C} = \mathbb{R}^m$  and  $q = (q_1, \dots, q_m) \in \mathcal{C}$ . Because each basis function  $\phi$  is normalized with respect to the energy norm, it has dimension of  $F^{-0.5}L^{-1.5}$  (F = Force, L = Length). The generalized coordinates have dimension  $F^{0.5}L^{0.5}$ , which is the square root of the dimension of energy. The kinematic differential equations imply that a solution  $p(s)$  is given when  $q$  is known and when initial conditions  $\vec{p}_0$  and  $\vec{d}_{k0}$  are known.

*Lemma 1:* The length of the  $i^{th}$  cable is calculated by the cable length functional:

$$L_i(q) = L_i[\kappa(q)] = \int_0^L g_i(\kappa(\sigma)) d\sigma \quad (12)$$

$$g_i(\kappa) = \sqrt{(r'_{i2})^2 + (1 - r_{i2}\kappa)^2} \quad (13)$$

*Proof:* The length of the cable is given by:

$$L_i(q) = \int_0^L \left\| \frac{d\vec{p}_i}{ds} \right\| ds \quad (14)$$

Calculating based on (1), and (2),

$$\left\| \frac{d\vec{p}_i}{ds} \right\| = \left\| \frac{d\vec{p}(s)}{ds} + r_{i2}(s) \frac{d\vec{d}_2(s)}{ds} + \frac{dr_{i2}(s)}{ds} \vec{d}_2(s) \right\| \quad (15)$$

Using (4), and (5),

$$\left\| \frac{d\vec{p}_i}{ds} \right\| = \left\| \vec{d}_1 + \vec{\kappa} \times \vec{r}_i + \frac{dr_{i2}(s)}{ds} \vec{d}_2(s) \right\| \quad (16)$$

Knowing that  $\vec{\kappa} \times \vec{r}_i$  is in the direction of  $-\vec{d}_1$  results in:

$$\left\| \frac{d\vec{p}_i}{ds} \right\| = \sqrt{(r'_{i2})^2 + (1 - r_{i2}\kappa)^2} = g_i(\kappa) \quad (17)$$

□

### 2.3. Perfect cable decoupling

We define the notion of perfectly decoupled cables to mean that  $n$  cable paths admit a choice of curvature modes so that the configuration space  $\mathcal{Q}$  may be partitioned into a direct sum:

$$\mathcal{Q} = \mathcal{Q}_1 \oplus \mathcal{Q}_2 \oplus \dots \oplus \mathcal{Q}_n \oplus \mathcal{Q}_{n+1} \quad (18)$$

such that each cable length depends only on one of the vector subspace:

$$\begin{aligned} L_1(q) &= L_1(q_1), & q_1 &\in \mathcal{Q}_1 \\ L_2(q) &= L_2(q_2), & q_2 &\in \mathcal{Q}_2 \\ &\vdots \\ L_n(q) &= L_n(q_n), & q_n &\in \mathcal{Q}_n \end{aligned} \quad (19)$$

The subspace  $\mathcal{Q}_{n+1}$  consists of the coordinates along curvature modes which do not affect the length of any cable. Thus, any configuration  $q$  may be written as a sum of components:

$$q = q_1 + q_2 + \dots + q_n + q_{n+1} \quad (20)$$

Due to the series (8) and the orthonormality of the basis  $B$ , the subspaces  $\mathcal{Q}_i$  are in direct one-to-one correspondence with subspaces  $V_i$  such that:

$$\kappa = \kappa_1 + \kappa_2 + \dots + \kappa_n + \kappa_{n+1} \quad (21)$$

These conditions state that the robot deformations can be partitioned into a sum of component deformations in which each component is associated with only a single cable or subset of cables. A natural question is “what cable path designs  $r_{i2}(s)$  admit such perfect

cable decoupling?” One obvious solution to the mathematical problem emerges, which is simply to locate the cable at zero radius to the backbone over all regions of the length except over a finite number of support regions. For example, divide the domain  $D = [0, L]$  into two subdomains  $D_1 = [0, a]$  and  $D_2 = [a, L]$ . If the cable shape function  $r_{12}(s)$  has support only on  $D_1$  and  $r_{22}(s)$  only on  $D_2$ , then the cables are perfectly decoupled. The corresponding spaces  $\mathcal{Q}_1$  and  $\mathcal{Q}_2$  are associated with curvature modes having support over the same subdomains, much like a serial kinematic structure. Practically speaking, any implementation of this strategy would require some means of routing a cable with zero radius to the backbone over some finite subset of the robot length or would require the placement of actuators at multiple places along the robot. Note that it is not enough to route cables from the base of a robot and have some cables terminate early before reaching the end. Doing so results in coupled cables, which motivated prior work on solving the coupled inverse kinematics problem [31].

#### 2.4. Approximate cable decoupling

Cables can be approximately decoupled by forcing the cable length functions to have gradients satisfying a condition of independence at a single point  $q \in \mathcal{Q}$ .

$$\nabla_q L_i \cdot e_j = 0, \quad \forall i \neq j \quad (22)$$

Define the first partial derivative as:

$$\frac{\partial L_i}{\partial q_j} \triangleq \int_0^L F_{ij}(r_i, r'_i, \kappa, \phi_j) ds \quad (23)$$

*Theorem 2:* The cables lengths are locally decoupled at  $q = 0$  and  $\kappa = 0$  if the following design condition applies to the cable routes:

$$\frac{r_i}{\sqrt{1 + (r'_i)^2}} = \alpha k_b \phi_i \quad (24)$$

The parameter  $\alpha \in \mathbb{R} \setminus 0$  is a free choice.

*Proof:* Using the chain derivative rule:

$$\left. \frac{\partial L_i}{\partial q_j} \right|_{\kappa=0} = \frac{\partial L_i}{\partial \kappa} \frac{\partial \kappa}{\partial q_j} \quad (25)$$

$$\frac{\partial \kappa}{\partial q_j} = \phi_j \quad (26)$$

$$\frac{\partial L_i}{\partial \kappa} = \int_0^L \frac{r_{i2}(\kappa r_{i2} - 1)}{\sqrt{(r'_{i2})^2 + (1 - \kappa r_{i2})^2}} ds \quad (27)$$

$$\left. \frac{\partial L_i}{\partial q_j} \right|_{\kappa=0} = \int_0^L \frac{r_{i2}(\kappa r_{i2} - 1)\phi_j}{\sqrt{(r'_{i2})^2 + (1 - \kappa r_{i2})^2}} ds \quad (28)$$

As an approximation, in the vicinity of  $\kappa = 0$  the  $\kappa r_{i2}$  term is  $\ll 1$ , hence:

$$\left. \frac{\partial L_i}{\partial q_j} \right|_{\kappa=0} = \int_0^L \frac{-r_{i2}\phi_j}{\sqrt{1 + (r'_{i2})^2}} ds \quad (29)$$

Now if we consider the Taylor expansion of  $F_{ij}$  about the point  $\kappa = 0$ ,

$$F_{ij} = \frac{r_{i2}\phi_j}{g_i(0)} + \mathcal{O}(\kappa) \quad (30)$$

Defining  $F_{ij0}$  to be the zeroth order (constant) term of the expansion, the independence of cable length  $i$  on mode  $j$  requires:

$$\int_0^L \frac{r_{i2}}{g_i(0)} \phi_j ds = 0 \quad (31)$$

By choice of  $r_{i2}$ , let:

$$\frac{r_{i2}}{g_i(0)} = \alpha k_b \phi_i \quad (32)$$

Then for all  $i \neq j$ :

$$\left. \frac{\partial L_i}{\partial q_j} \right|_{\kappa=0} = \alpha < \phi_i, \phi_j >_{k_b} = 0 \quad (33)$$

□

The parameter  $\alpha$  is a scale parameter and has dimension  $F^{-0.5} L^{0.5}$  to ensure dimensional homogeneity of (18). As one example of a pair of orthogonal modes, consider the following choices:

$$\begin{aligned} \phi_1 &= \frac{1}{\sqrt{L k_b}} \\ \phi_2 &= \frac{\sqrt{2}}{\sqrt{L k_b}} \cos\left(\frac{\pi s}{L}\right) \end{aligned} \quad (34)$$

which satisfy the orthogonality condition for any robot having uniform (constant in arc length) flexural rigidity  $k_b$ . The first curvature mode corresponds to circular bending (i.e., “constant curvature”), and the cable shape  $r_{12}$  is the usual straight cables at a constant radius to the backbone. The cable shapes  $r_{i2}$ , in a geometric sense independent of scale, are determined by the dimensionless group:

$$\Pi_1 = \frac{\alpha \sqrt{k_b}}{L^{1.5}} \quad (35)$$

For small values of  $\Pi_1$ , the cable shapes mimic the right-hand side of (21), i.e.,  $r_{i2} \approx \alpha k_b \phi_i$ . As  $\Pi_1$  increases, the cable shape begins to change substantially (Figure 2.1). The solutions found to (24) for  $\phi_2$  as in (34) demonstrate a critical value of  $\alpha$  at which the cable path folds back on itself, implying that the robot must be sufficiently slender for this design approach to be practical. “Folded” cable paths may be difficult to support mechanically and may also cause high cable friction.



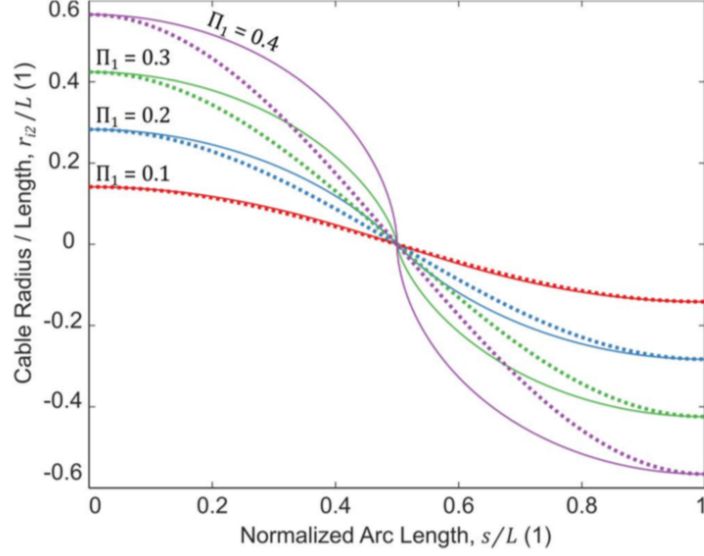


Figure 2.1. Cable shapes for  $\phi_2$  described by (34). Solid lines depict the cable paths solving the design condition of Theorem 2. Dashed lines correspond to the right side of (24). The shape and scale of the cable path, normalized by the length of the backbone, is determined by the dimensionless parameter  $\Pi_1$ . At a critical value near  $\Pi_1 = 0.4$ , the cable path crosses the backbone of the robot nearly perpendicularly.

The critical value of  $\Pi_1$  depends on the specific functional basis chosen. For example, if instead  $\phi_2$  is a linear function,

$$\phi_2 = \frac{\sqrt{3}}{\sqrt{Lk_b}} \left(1 - \frac{2s}{L}\right) \quad (36)$$

then the solution  $r_{22}$  can be found by ansatz as  $r_{22} = mx + b$ , where the parameters are given by:

$$m = -\frac{2\sqrt{3}\Pi_1}{\sqrt{1 - 12\Pi_1^2}} \quad (37)$$

$$b = \frac{\sqrt{3}\Pi_1 L}{\sqrt{1 - 12\Pi_1^2}} \quad (38)$$

The critical value for linear cable paths is therefore,

$$\Pi_1^* = \sqrt{1/12} \approx 0.2887 \quad (39)$$

The decoupled cable design also results in a simple relationship between the tension in the cables and the resulting robot shapes if the deflections remain small. With orthonormal curvature modes and cable routes designed according to the conditions of Theorem 2, the generalized coordinates and the cable tension increments  $t_i$  (above the pretension) are approximately related by:

$$t_i \approx \frac{2q_i}{\alpha_i} \quad (40)$$

*Proof:* consider static equilibrium on a section. The total internal moment in the backbone must be equal to  $m$ , calculated as follows:

$$m = \sum_{i=1}^n t_i r_i \cos \gamma_i \quad (41)$$

The angle  $\gamma_i$  is the angle between the tangent to the cable path cable and the tangent to the backbone. For small curvatures it may be approximated as:

$$\cos \gamma_i \approx \frac{1}{\sqrt{1 + (r'_i)^2}} \quad (42)$$

Based on assumption (3), the elastic energy is:

$$E = \frac{1}{2} \int_0^L m \kappa \, ds = \frac{1}{2} \sum_{i=1}^{\infty} q_i^2 \quad (43)$$

By application of the cable design condition, calculation of the moment in terms of the cable tensions, and direct substitution,

$$E \approx \frac{1}{2} \int_0^L \left( \sum_{i=1}^n \frac{t_i r_i(s)}{\sqrt{1 + (r'_i)^2}} \right) \left( \sum_{i=1}^{\infty} q_i \phi_i(s) \right) ds = \frac{1}{2} \sum_{i=1}^n c_i t_i q_i \quad (44)$$

Where

$$c_i = \alpha_i < \phi_i, \phi_i >_{k_b} = \alpha_i \quad (45)$$

Then the cable tension is calculated as:

$$t_i \approx \frac{2}{c_i} \frac{\partial E}{\partial q_i} \quad (46)$$

The result (40) follows by direct calculation.

This result demonstrates that the interpretation of the scale parameter  $\alpha_i$  is approximately the inverse of half the cable tension required to create a unit of deformation along the coordinate  $q_i$ . A unit deformation along  $q_i$  stores one unit of elastic energy by virtue of its definition, with the unit of measure determined by the units of  $\phi_i$  and  $k_b$ .

The orthogonality of the curvature basis also provides a convenient calculation of the component of the cable tensions due to the elastic forces for an arbitrary configuration of the robot, which follows directly from Theorem 3 and the definition of the energy inner product:

$$t_i \approx \frac{2}{\alpha_i} < \kappa, \phi_i >_{k_b} \quad (47)$$

If the cables are pretensioned, then this calculated tension due to the elastic internal forces is simply superposed on the pretension to arrive at the final cable tension. Note that this approximate calculation should not be understood as a method of calculating the tensions that will produce a given shape except when prior knowledge is available to suggest that the shape is indeed the feasible result of the cable tensions, since in general, an arbitrary specification of the shape would require an infinite number of cables to achieve and yet (47) could be applied regardless of this fact.

The preceding analysis also implies that in a traditionally designed cable-driven continuum robot having only a single pair of cables that antagonistically actuate a constant curvature mode, the actuating cable has little effect on the apparent stiffness of higher-order curvature modes. Curvature along these higher-order modes does not substantially change the length of the actuating cable, at least in the sense of small deflections, and the tension in the cable is approximately independent of these other modes.

## Chapter 3. Experimental Validations

### 3.1. Cable stiffening design considerations

<sup>1</sup> The approximate cable decoupling condition suggests a means of modifying the natural compliance of cable-driven robots through the addition of cables that are routed so that the cable lengths couple weakly to the actuated curvature modes of the robot. Using the approach outlined in the flowchart of Figure 3.1, we designed a robot having an actuated constant curvature mode and a stiffened sinusoidal curvature mode using an additional pair of cables routed in the appropriate shape  $r_{i2}(s)$  which was generated by  $\phi_2$  as in (34). These additional cables are pretensioned and locked off. In other words, the additional stiffening cables are unactuated, and the length of cable is constant. The constant curvature actuating cables are a single cable loop driven by a manually controlled, self-locking worm wheel which drives a short segment of a timing belt to which the cables are attached.

---

<sup>1</sup>Some portions of Chapter 3 were previously published as: "Molaei, P., Pitts, N. A., Palardy, G., Su, J., Mahlin, M. K., Neilan, J. H., Gilbert, H. B. (2022). Cable Decoupling and Cable-Based Stiffening of Continuum Robots. IEEE Access, 10, 104852-104862."

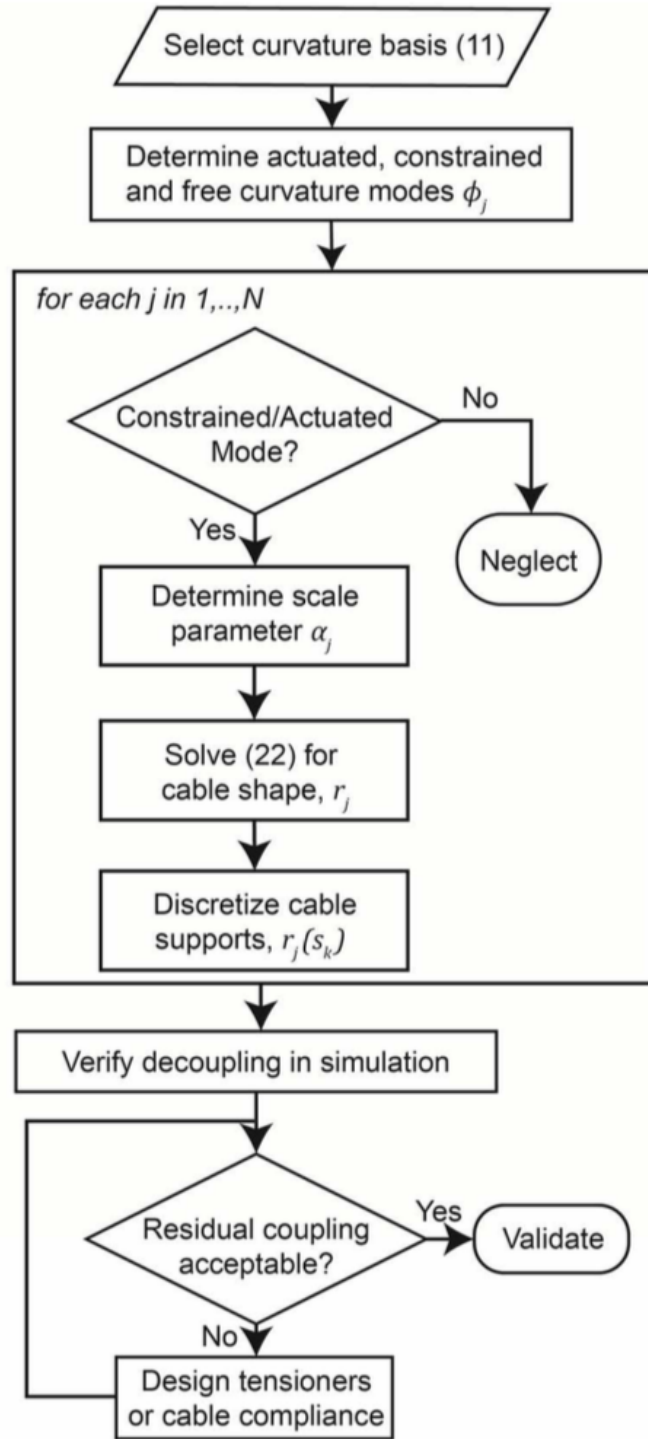


Figure 3.1. Flowchart describing the design approach for producing multiple decoupled cables along independent elastic curvature modes.

### 3.2. Prototype design

<sup>1</sup> The backbone of the robot is made from a 2-ply carbon fiber (CF)/epoxy laminate, manufactured by resin infusion, with a final thickness of 0.59 mm (Composite Environments, Wausau, WI, USA). The CF is a 3K plain weave fabric and was stacked in a symmetric layup with respect to the laminate's geometric mid-plane. The cables are made from commercially available braided ultra-high molecular weight polyethylene fishing line with a strength of 10 lb test (Stealth Smooth 8, 10lb, SpiderWire, CA, USA). 7 individual tendon support structures and the mounting base frame were manufactured and printed using a FDM 3D printer and Nylon filament. The robot's dimensions are described in Table 3.1 and shown in Figure 3.2 and the cable support radii are described in Table 3.2.

Table 3.1. Prototype robot design parameters.

Parameter	Symbol	Value
Backbone length	L	270 mm
Backbone height	h	60 mm
Backbone thickness	t	0.59 mm
No. of tendon supports	N	7
tendon support spacing	$\Delta L$	45 mm

Table 3.2. Prototype cable support locations and radii.

Support index, $i$	Support location, $s_i(mm)$	$r_{12}(mm)$	$r_{22}(mm)$
1	0	30.0	25.0
2	45	30.0	21.7
3	90	30.0	12.5
4	135	30.0	0
5	180	30.0	-12.5
6	225	30.0	-21.7
7	270	30.0	-25.0

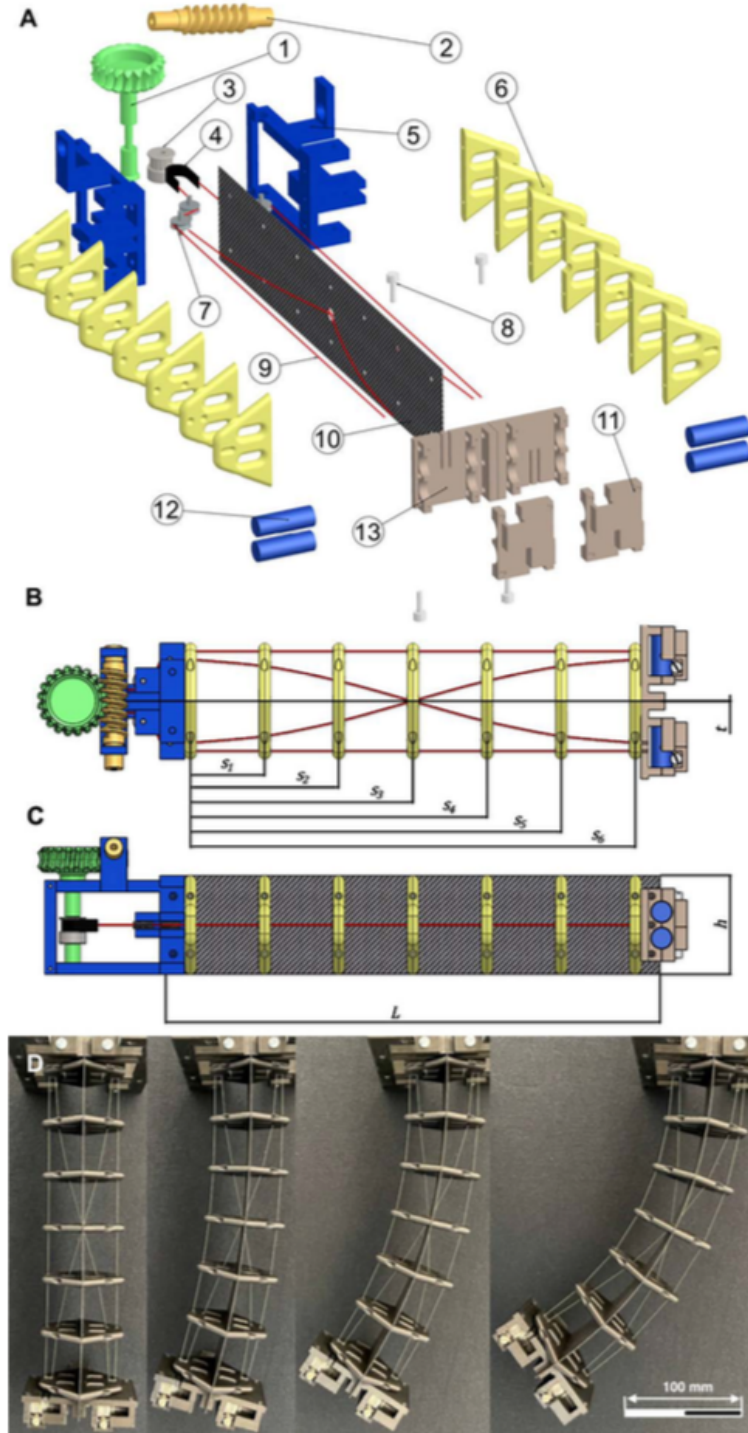


Figure 3.2. A. Exploded view. ① worm gear ② worm ③ timing pulley ④ timing belt segment ⑤ base frame ⑥ cable supports ⑦ cable routing pulleys ⑧ fasteners ⑨ cables ⑩ carbon fiber backbone ⑪ tensioner clamp ⑫ tensioner barrel ⑬ tensioner housing B. Top view (assembled). C. Side view (assembled). D. Sequence (left-to-right) of increasing curvature caused by turning the worm. All cables are pretensioned.



To make the robot prototype as light as possible topological optimization and FEM modeling was conducted on the design parameters of the cable support structures in order to find the optimum combination for shape and load resistance across the length of the robot.

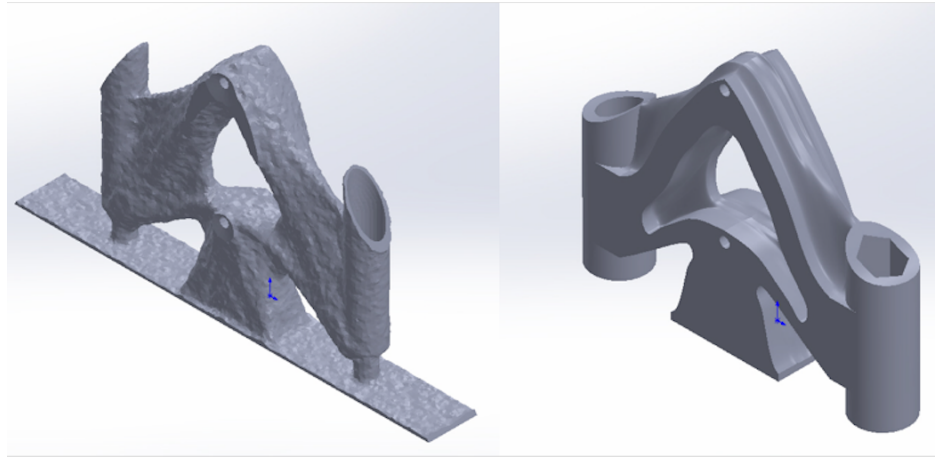


Figure 3.3. Topology optimization result of cable supports. Mesh view on the left and smoothed design on the right.

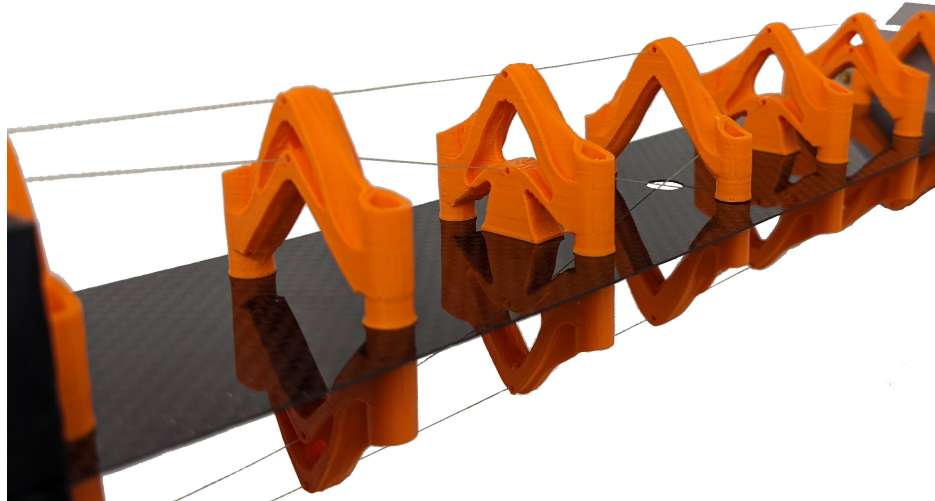


Figure 3.4. Topology optimized 3D printed cable support assembled on the backbone.

### 3.3. Kinematic simulations

To verify that the approximate decoupling at zero curvature is a practical design condition, we performed the evaluation of the residual coupling, as shown in the flowchart, using a kinematic simulation of a cable-driven robot using the constant and cosine curvature modes. The robot is assumed to be actuated using the constant radius cables, which apply a generalized force that tends to actuate the constant curvature mode if no other constraints are present. The backbone curve is simulated according to the piecewise constant curvature method described by Webster and Jones [32]. The cable lengths for each of the four cables (two antagonistic pairs) are modeled by the sum of the distances between the cable support holes. The results from the simulation for the prototype design parameters are shown in the Figure 3.5., the total path length for the stiffening cables changes only by 0.88 mm over a change in robot bending angle from  $0^\circ$  to  $90^\circ$ . The sum of the actuating cable lengths changes by a similar amount. This amount of residual coupling was deemed acceptable without additional design effort that coupling, such as via the introduction of cable tensioners or compliance in the cables or cable supports.

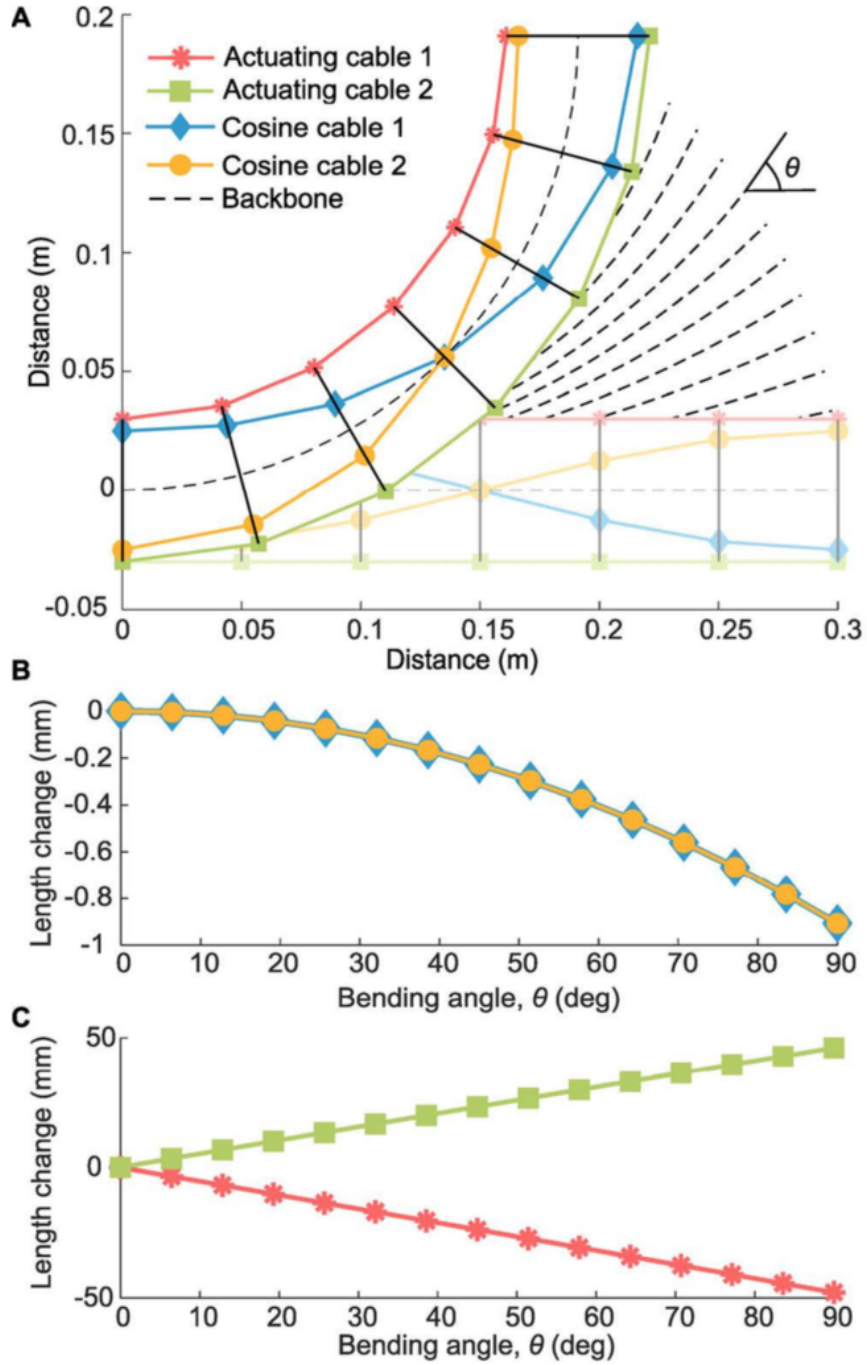


Figure 3.5. Simulation of constant curvature bending of the backbone. Cable supports are treated as rigid bodies, and cable lengths are calculated by the sum of point-to-point Euclidean distance between the supports. B. Length change of the stiffening cable paths as the robot bends. C. Length change of the actuating cable paths as the robot bends.

### 3.4. Prototype stiffness measurements

To assess the influence of the stiffening cables on the mechanical performance of the robot, we used an industrial robot manipulator (UR5e, Universal Robots) to produce controlled displacements of the robot backbone while measuring the reaction force with a load cell (LCMFL-20N, OMEGA, Norwalk, CT, USA). The experimental setup is depicted in Figure 3.8. Analog voltage samples were recorded at 30 S/s. The base of the cable-driven continuum robot was fixed to a support structure mounted to the same table as the UR5e robot base. The UR5e was programmed to displace the continuum robot by contacting it at each of the cable support structures in sequence. The maximum displacement of each support disc was approximately 5 mm. The same controlled displacement profile was used for all trials. The motion of the UR5e end-effector was tracked by a three-camera OptiTrack motion capture system set to acquire frames at 30 S/s. After data acquisition, a manual coordinate system rotation was performed to align the displacement during contacts to the x-axis of the coordinate system. The peaks in the x-displacement and the force time series were identified manually and a region around each peak of length 300 samples was segmented to produce a force vs. displacement response for contact forces at the cable support structure positions. The entire experiment was repeated three times, and a linear model of the following form was fit to the data by least squares regression

$$F_{kl} = \beta_k x + \eta_{kl} \quad (48)$$

The index  $k = 1, \dots, 7$  indicates the contact location and the index  $l = 1, 2, 3$  indicates the experimental repetition.  $\beta_k$  are the stiffnesses observed at each contact location (i.e., both the force and displacement are measured at the contact location),  $x$  is the rotated

end-effector coordinate of the UR5, and  $\eta_{kl}$  is a contact-location and repetition-dependent bias term. Time series data from one trial of the experiment with all cables pretensioned is shown in Figure 3.6. The segmentations of each trial were used to construct the linear regression model described by (48). The stiffness parameters  $\beta_k$  are shown for each pretensioning case and at each location of applied force in Figure 3.6. Statistically significant differences in the stiffness of the robot are evident depending on which cables are pretensioned and which are slacked. The stiffness is greatest at each location when all cables are pretensioned, indicating that, at least for the design and range of pretensions tested, it is not possible for an increase in pretension to result in a decrease in observable stiffness.

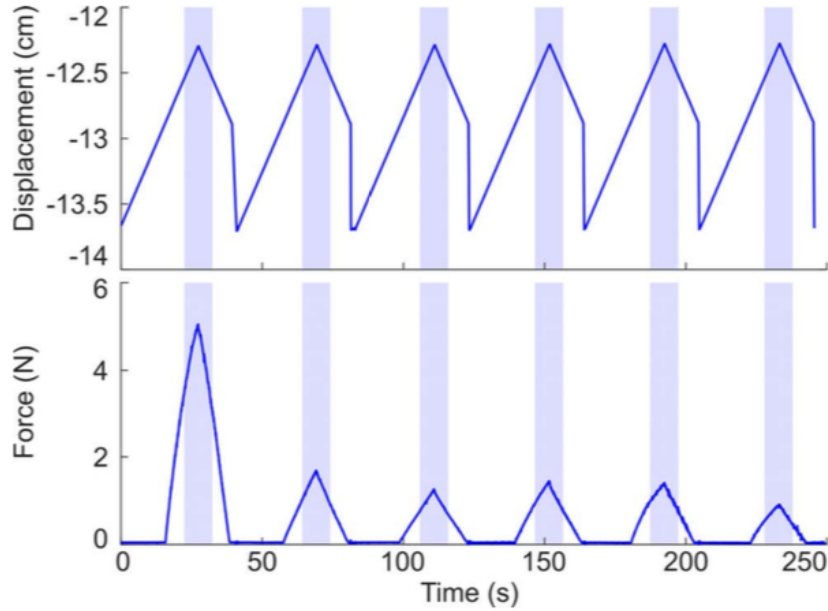


Figure 3.6. Force and displacement data captured during trial 1 of the case with all cables pretensioned. The manual segmentation of the data is overlaid as blue shading. Contact between the UR5 and the robot under test exists whenever the force is nonzero.

The results shown in Figure 3.7 demonstrate that the end-effector stiffness, which is measured at the furthest point from the fixed base, is similar between cases N (no cables) and C (stiffening cables only). This is expected because a force applied at the end-effector will tend to produce deformation along the lowest order mode more than the higher modes. In the case of no cables, the deflection is approximately a third order polynomial with distance (the classic Euler-Bernoulli beam solution for cantilevered loads applied on uniform beams). The cosine-shaped cables are designed to match a mode which is orthogonal to the lowest order constant-curvature mode. On the other hand, when all cables are pretensioned, the response of the structure is substantially different than in any of the other conditions. Most notably, the end-effector stiffness is increased by approximately a factor of 14 when compared to case N and a factor of 10 when compared to case A, which is the most common case found in prior literature. However, at the midpoint of the robot, the stiffness increase is only a factor of 3.45 times higher than case N and 5 times higher than case A.

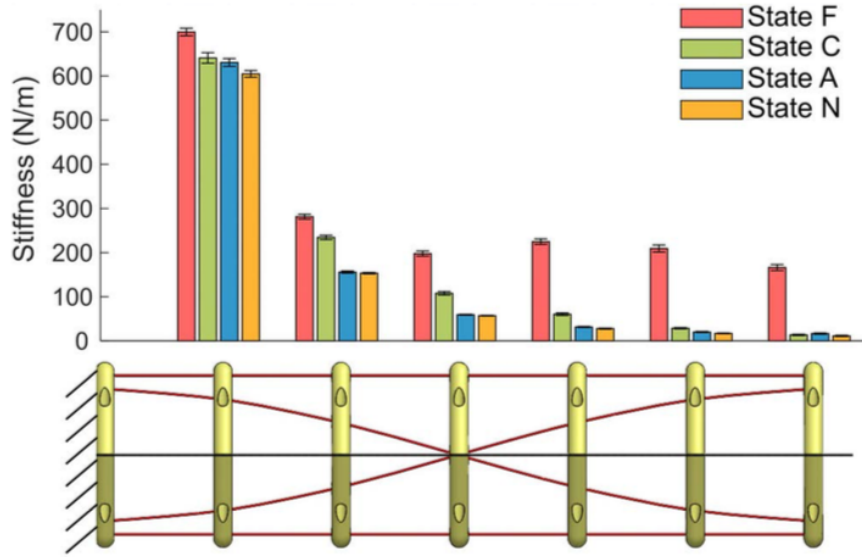


Figure 3.7. Stiffness along the length of the cable-driven robot with one fixed boundary condition. Bars indicate stiffness and are grouped by physical location of the measurement (at each of the cable support structures). Whiskers indicate the 95 % confidence intervals of the parameter estimates. Stiffness is measured across the factor of condition of cable pretensioning with the factors being (N) no cables pretensioned, (A) actuating cables only pretensioned, (C) stiffening cables only pretensioned, and (F) all cables pretensioned.



Figure 3.8. Experimental setup for stiffness characterization of the cable-driven continuum robot for contact forces applied at different locations along the robot.



## Chapter 4. Discussion

<sup>1</sup> When the cables are designed according to Theorem 2, the cable lengths are approximately decoupled, and each cable’s tension couples predominantly to the mode for which it is designed, as illustrated clearly by (40). The implication of this is that even though perfect decoupling is not possible, small amounts of stretch allowed in the cables and cable support structures means that all cables, even those which are tied off and have an ostensibly fixed length, may remain taut even when the robot undergoes large deflections.

The stiffness of the cable-driven robot is modified substantially by the introduction of the additional stiffening cables which are designed according to the conditions of Theorem 2. In particular, the distribution of stiffness is altered fundamentally from the typical inverse cube law for the stiffness of a cantilevered structure. An interesting observation is that when all cables are pretensioned, the stiffness at the fourth cable support is higher than the stiffness at the third support, which is atypical for a cantilevered structure. It is noteworthy that this is the location where the stiffening cable crosses over the backbone. This result is expected, and one way to explain it is that the next higher mode in the orthogonal trigonometric series is  $\cos\left(\frac{2\pi s}{L}\right)$ , over which the stiffening cable has little influence. For small deflections, this next mode is associated with deflections that are the second integral of the curvature, which has a maximum exactly at the point where the stiffness is measured to be a minimum.

---

<sup>1</sup>Some portions of Chapter 4 were previously published as: "Molaei, P., Pitts, N. A., Palardy, G., Su, J., Mahlin, M. K., Neilan, J. H., Gilbert, H. B. (2022). Cable Decoupling and Cable-Based Stiffening of Continuum Robots. IEEE Access, 10, 104852-104862."

Since the orthogonality condition in Definition 3 is general, one avenue for future work is to understand how the choice of basis affects the properties of the resulting robot. The orthogonal trigonometric sequence is not the only orthogonal function sequence which can form a curvature basis. For example, the cosine and linear cable shapes are two of infinitely many alternatives for cable designs that are orthogonal to a straight cable. Future work is needed to determine the advantages and disadvantages to specific selections of the basis.

Although not quantified experimentally, we observed through direct manipulation of the robot by hand that in the experimental condition with all cables pretensioned, the stiffness of the end-effector to applied torques in the plane of bending was vastly increased in comparison to the case in which only the actuating cables are pretensioned.

One limitation of the overall strategy is that the additional cables increase the compressive preload in the backbone member. At some critical load, the backbone itself may buckle between the cable tie off points. On the other hand, the buckling modes are themselves deformations of the backbone which may be controlled by the additional cables. The balance of these effects should also be investigated in future work.

## Chapter 5. Conclusion

Cable-driven continuum manipulators provide interesting solutions to the problems that require flexibility and adaptability in unstructured and uncertain environments. The novel but simple approach that was presented enables large changes in structural stiffness or actuation of independent mode shapes. The designed prototype demonstrated a 10x increase in stiffness at the endpoint, with substantial improvement in torsional rigidity compared to traditional tendon routing. Continuum robotic manipulators, given their possibly infinite-dimensional deformation characteristics, provide a continuing challenge in modeling and control. This work provides a strategy and next steps in addressing the problem at hand, towards a methodology to address uncontrolled deformation of these mechanisms.

## Appendix A. Kinematic Simulations MATLAB Code

```
L = 0.30; N = 7;

x = linspace(0, L, N);

dx = x(2) - x(1);

pos = @(T) T(1:3, 4);

colors = {'r', 'g', 'b', 'm', 'c', 'b'};

vec2hom = @(x) [x; 1];

hom2vec = @(x) x(1: 3);

tendon(1).rT = 0.030*[0; 1; 0]*ones(1, N);

tendon(2).rT = -0.030*[0; 1; 0]*ones(1, N);

tendon(3).rT = [zeros(1, N); ...

               [0.0250    0.0216    0.0125    0.0000

                -0.0125   -0.0216   -0.0250]; ...

               zeros(1, N)];

tendon(4).rT = -[zeros(1, N); ...

                [0.0250    0.0216    0.0125    0.0000

                 -0.0125   -0.0216   -0.0250]; ...

                zeros(1, N)];

theta = linspace(0, pi/2, 10);

for jj = 1:numel(theta)

    u = theta(jj)/L;

    %run the forward kinematics for the tendon supports
```

```

X = [0, -u, 0, 1; ...
      u, 0, 0, 0; ...
      0, 0, 0, 0; ...
      0, 0, 0, 0];

for kk = 1:numel(tendon)
    deformed.tendon(kk).rT = zeros(size(tendon(kk).rT));
    deformed.tendon(kk).rT(:, 1) = tendon(kk).rT(:, 1);
end

p = zeros(3, numel(x));

for kk = 2:numel(x)
    i = kk-1;
    T{i} = expm(X*dx*i);
    p(:, kk) = pos(T{i});
end

for kk = 1:numel(tendon)
    for ll = 2:numel(x)
        i = ll-1;
        deformed.tendon(kk).rT(:, ll) = hom2vec(T{i}*
            vec2hom(tendon(kk).rT(:, ll)));
    end
end

plot(p(1, :), p(2, :), 'k-', 'LineWidth', 2); hold on;

```

```

for kk = 1:numel(tendon)

    plot(deformed.tendon(kk).rT(1, :), deformed.tendon(kk).
        rT(2, :), [colors{kk}, '-x']);

end

for kk = 1:numel(tendon)

    deformed.tendon(kk).L = sum(vecnorm(diff(deformed.
        tendon(kk).rT, 1, 2), 2, 1));

end

for kk = 1:numel(tendon)

    text(0.02, 0.15-0.01*kk, [sprintf('Tendon %d Length: ',
        kk) sprintf('%3.2f', 1000*deformed.tendon(kk).L), '
        mm']);

end

text(0.02, 0.15+0.01,[ 'Tendon 1 Loop Length: ', sprintf('
        %3.2f', 1000*(deformed.tendon(1).L+deformed.tendon(2).L)
        ), ' mm']);

axis equal
xlim([0, 0.35])
ylim([-0.05, 0.25])

hold off

pause

end

```

## Appendix B. Publication Information

### RESEARCH ARTICLE

## Cable Decoupling and Cable-Based Stiffening of Continuum Robots

PARSA MOLAEI<sup>1</sup>, (Graduate Student Member, IEEE), NEKITA A. PITTS<sup>1</sup>,  
GENEVIEVE PALARDY<sup>1</sup>, JI SU<sup>2</sup>, MATTHEW K. MAHLIN<sup>3</sup>, JAMES H. NEILAN<sup>4</sup>,  
AND HUNTER B. GILBERT<sup>1</sup>, (Member, IEEE)

<sup>1</sup>Department of Mechanical and Industrial Engineering, Louisiana State University, Baton Rouge, LA 70803, USA

<sup>2</sup>Advanced Materials and Processing Branch, Research Directorate, NASA Langley Research Center, Hampton, VA 23681, USA

<sup>3</sup>Structural Mechanics and Concepts Branch, Research Directorate, NASA Langley Research Center, Hampton, VA 23681, USA

<sup>4</sup>Space Technology and Exploration Directorate, NASA Langley Research Center, Hampton, VA 23681, USA

Corresponding author: Hunter B. Gilbert (hbgilbert@lsu.edu)

This work was supported in part by the Louisiana Space Grant Consortium with funding provided by the National Aeronautics and Space Administration under Grant 80NSSC20M0110, in part by the Louisiana Board of Regents under Contract LEQSF(2020-24)-LaSPACE, and in part by the United States National Science Foundation under Award 2133019.

**ABSTRACT** Cable-driven continuum robots, which are robots with a continuously flexible backbone and no identifiable joints that are actuated by cables, have shown great potential for many applications in unstructured, uncertain environments. However, the standard design for a cable-driven continuum robot segment, which bends a continuous backbone along a circular arc, has many compliant modes of deformation which are uncontrolled, and which may result in buckling or other undesirable behaviors if not ameliorated. In this paper, we detail an approach for using additional cables to selectively stiffen planar cable-driven robots without substantial coupling to the actuating cables. A mechanics-based model based on the planar Cosserat equations is used to find the design conditions under which additional cables can be routed without coupling of the cable lengths for small deformations. Simulations show that even for relatively large deformations, coupling remains small. A prototype is evaluated, and it is demonstrated that the compliance of the robot is substantially modified relative to the same robot without stiffening cables. Additional stiffening cables are shown to increase the end-effector output stiffness by a factor of approximately 10 over a typical design with actuating cables.

**INDEX TERMS** Tendon/wire mechanism, flexible robots, continuum robots, compliant joint mechanism.

### I. INTRODUCTION

Human space exploration is an essential mission of the National Aeronautics and Space Administration (NASA). The development of large and sustainable structures in space and for planetary habitats has been identified as one of the key enabling technologies as the next strategic thrust in space technology advancement. Various in-space assembly technologies have been developed for making large space assets at NASA Langley Research Center. A cable-driven compliant space robotic technology has demonstrated unique capabilities and advantages in terms of flexibility, durability, and remote adjustability. The performance of the system can

be optimized by the design of configuration and the selection of cable materials through modeling and experimental validation.

#### A. IN-SPACE ASSEMBLY

Advancing human space exploration entails developing larger and more sustainable structures in space and on other worlds requiring in-space manufacturing, assembly, and servicing. Identified as the next strategic thrust for NASA, In-space Assembly Servicing and Manufacturing (ISAM) offers key possibilities by freeing a mission from the restrictions of mass and volume of current launch vehicles. It is also crucial to consider how to optimize assembly methods and agents being used to diversify what capabilities they must allow for a broad range of applications, minimizing launch cost.

The associate editor coordinating the review of this manuscript and approving it for publication was Yangmin Li<sup>1</sup>.

## Bibliography

- [1] Mazzolai, B., Margheri, L., Cianchetti, M., Dario, P., Laschi, C. (2012). Soft-robotic arm inspired by the octopus: II. From artificial requirements to innovative technological solutions. *Bioinspiration biomimetics*, 7(2), 025005.
- [2] Camarillo, D. B., Carlson, C. R., Salisbury, J. K. (2009). Configuration tracking for continuum manipulators with coupled tendon drive. *IEEE transactions on robotics*, 25(4), 798-808.
- [3] Moses, M. S., Murphy, R. J., Kutzer, M. D., Armand, M. (2015). Modeling cable and guide channel interaction in a high-strength cable-driven continuum manipulator. *IEEE/ASME Transactions on Mechatronics*, 20(6), 2876-2889.
- [4] Mahlin, M., Wagner, R. L., Dorsey, J., Jones, T. C. (2020). Tendon-actuated lightweight in-space MANipulator (TALISMAN) Hinge joint structural. In *ASCEND 2020* (p. 4251).
- [5] Buckingham, R., Graham, A. (2012). Nuclear snake-arm robots. *Industrial Robot: An International Journal*.
- [6] Walker, I. D., Hannan, M. W. (1999, September). A novel "elephant's trunk" robot. In *1999 IEEE/ASME International Conference on Advanced Intelligent Mechatronics* (Cat. No. 99TH8399) (pp. 410-415). IEEE.
- [7] Trivedi, D., Rahn, C. D., Kier, W. M., Walker, I. D. (2008). Soft robotics: Biological inspiration, state of the art, and future research. *Applied bionics and biomechanics*, 5(3), 99-117.
- [8] Robinson, G., Davies, J. B. C. (1999, May). Continuum robots-a state of the art. In *Proceedings 1999 IEEE international conference on robotics and automation* (Cat. No. 99CH36288C) (Vol. 4, pp. 2849-2854). IEEE.
- [9] Burgner-Kahrs, J., Rucker, D. C., Choset, H. (2015). Continuum robots for medical applications: A survey. *IEEE Transactions on Robotics*, 31(6), 1261-1280.
- [10] Bajo, A., Goldman, R. E., Wang, L., Fowler, D., Simaan, N. (2012, May). Integration and preliminary evaluation of an insertable robotic effectors platform for single port access surgery. In *2012 IEEE international conference on robotics and automation* (pp. 3381-3387). Ieee.
- [11] Loeve, A., Breedveld, P., Dankelman, J. (2010). Scopes too flexible... and too stiff. *IEEE pulse*, 1(3), 26-41.



- [12] Doggett, W. (2002, March). Robotic assembly of truss structures for space systems and future research plans. In *Proceedings, IEEE Aerospace Conference* (Vol. 7, pp. 7-7). IEEE.
- [13] J. Lymer, “NASA’s dragonfly program: Commercialized robotics— Enabling a new generation of evolvable, resilient assets in orbit,” in *Proc. 35th Space Symp.*, 2019, pp. 1–6.
- [14] Patane, S., Joyce, E. R., Snyder, M. P., Shestopole, P. (2017). Archinaut: In-space manufacturing and assembly for next-generation space habitats. In *AIAA SPACE and astronautics forum and exposition* (p. 5227).
- [15] Bowman, L. M., Belvin, W. K., Komendera, E. E., Dorsey, J. T., Doggett, B. R. (2018, July). In-space assembly application and technology for NASA’s future science observatory and platform missions. In *Space Telescopes and Instrumentation 2018: Optical, Infrared, and Millimeter Wave* (Vol. 10698, pp. 690-708). SPIE.
- [16] Mukherjee, R., Siegler, N., Thronson, H., Aaron, K., Arenberg, J., Backes, P., ... Wood, J. (2019). When is it worth assembling observatories in space?. *Bulletin of the American Astronomical Society*, 51(7), 50.
- [17] Chen, L. H., Kim, K., Tang, E., Li, K., House, R., Zhu, E. L., ... Jung, E. (2017). Soft spherical tensegrity robot design using rod-centered actuation and control. *Journal of Mechanisms and Robotics*, 9(2).
- [18] Jones, J. A., Wu, J. J. (1999, November). Inflatable rovers for planetary applications. In *Mobile Robots XIV* (Vol. 3838, pp. 63-68). SPIE.
- [19] Booth, J. W., Shah, D., Case, J. C., White, E. L., Yuen, M. C., Cyr-Choiniere, O., Kramer-Bottiglio, R. (2018). OmniSkins: Robotic skins that turn inanimate objects into multifunctional robots. *Science Robotics*, 3(22), eaat1853.
- [20] Peck, M. (2016). Soft-Robotic Rover with Electrodynamic Power Scavenging (No. HQ-E-DAA-TN62782).
- [21] Holschuh, B. T., Newman, D. J. (2016). Morphing compression garments for space medicine and extravehicular activity using active materials. *Aerospace medicine and human performance*, 87(2), 84-92.
- [22] Laschi, C., Cianchetti, M. (2014). Soft robotics: new perspectives for robot bodyware and control. *Frontiers in bioengineering and biotechnology*, 2, 3.
- [23] Degani, A., Choset, H., Wolf, A., Zenati, M. A. (2006, May). Highly articulated robotic probe for minimally invasive surgery. In *Proceedings 2006 IEEE International Conference on Robotics and Automation, 2006. ICRA 2006.* (pp. 4167-4172). IEEE.

- [24] Manti, M., Cacucciolo, V., Cianchetti, M. (2016). Stiffening in soft robotics: A review of the state of the art. *IEEE Robotics Automation Magazine*, 23(3), 93-106.
- [25] Wang, R., Li, S., Li, Y. (2022). A suspended cable-driven parallel robot with articulated reconfigurable moving platform for Schönflies motions. *IEEE/ASME Transactions on Mechatronics*, 27(6), 5173-5184.
- [26] Rucker, D. C., Webster III, R. J. (2011). Statics and dynamics of continuum robots with general tendon routing and external loading. *IEEE Transactions on Robotics*, 27(6), 1033-1044.
- [27] Rao, P., Peyron, Q., Lilge, S., Burgner-Kahrs, J. (2021). How to model tendon-driven continuum robots and benchmark modelling performance. *Frontiers in Robotics and AI*, 7, 630245.
- [28] Chitalia, Y., Jeong, S., Deaton, N., Chern, J. J., Desai, J. P. (2020). Design and kinematics analysis of a robotic pediatric neuroendoscope tool body. *IEEE/ASME Transactions on Mechatronics*, 25(2), 985-995.
- [29] Oliver-Butler, K., Till, J., Rucker, C. (2019). Continuum robot stiffness under external loads and prescribed tendon displacements. *IEEE Transactions on Robotics*, 35(2), 403-419.
- [30] Chirikjian, G. S., Burdick, J. W. (1994). A modal approach to hyper-redundant manipulator kinematics. *IEEE Transactions on Robotics and Automation*, 10(3), 343-354.
- [31] Jones, B. A., Walker, I. D. (2006). Practical kinematics for real-time implementation of continuum robots. *IEEE Transactions on Robotics*, 22(6), 1087-1099.
- [32] Webster III, R. J., Jones, B. A. (2010). Design and kinematic modeling of constant curvature continuum robots: A review. *The International Journal of Robotics Research*, 29(13), 1661-1683.

## **Vita**

Parsa Molaei, born in Tehran, Iran, after graduating from High School in 2013, he enrolled in Sharif University of Technology in Tehran, Iran, where he earned a Bachelor of Science degree in Mechanical Engineering in Spring 2018. He began his doctoral research in the Department of Mechanical and Industrial Engineering at Louisiana State University in Baton Rouge, USA, and worked in the Innovation in Control and Robotics Engineering (iCORE) Lab as a graduate researcher with the focus on the stability of the soft/continuum robots.